Influence of Proximal Side Mutations on the Molecular and Electronic Structure of Cyanomet Myoglobin: An ^{1}H NMR Study†

Yuyang Wu,‡ Ellen Y. T. Chien,§ Stephen G. Sligar,§ and Gerd N. La Mar*,‡

Department of Chemistry, University of California, Davis, California 95616, and Department of Chemistry, Biochemistry, Physiology and Biophysics, The Beckman Institute of Advanced Science and Technology, University of Illinois, Urbana-Champaign, Illinois 61801

Received November 18, 1997; Revised Manuscript Received March 6, 1998

ABSTRACT: A series of proximal side mutants of sperm whale metmyoglobin (metMb) that involves residues which provide hydrogen bonds to the axial His and heme have been prepared, and the CO binding and solution molecular and electronic structure has been investigated by ^{1}H NMR. These include Ser92(F7), whose O_γ serves as a hydrogen-bond acceptor to the axial His ring $N_\delta H$ and whose $O_\gamma H$ serves as hydrogen-bond donor to the 7-propionate carboxylate, and His97(FG3) whose ring provides the other hydrogen-bond donor to the 7-propionate carboxylate. 2D NMR data on the S92A-metMbCN, S92P-metMbCN and H97F-metMbCN show that the distal structure is completely conserved and that proximal side structural changes are highly localized. For the S92A-metMbCN, altered dipolar contacts to the F-helix backbone show that the axial His imidazole has rotated clockwise by ∼10° relative to a stationary heme, while in H97F-metMbCN, the altered heme-E helix backbone contacts reveal that the heme has rotated counterclockwise by ∼3° relative to a conserved axial His. The pattern of axial His rotation was qualitatively predicted by energy minimization calculations. The assignments and conserved structural elements allow the determination of a set of magnetic axes whose major magnetic axis is unchanged with respect to WT and confirms that local distal, and not proximal, interactions control the orientation of the major magnetic axis and, by inference, the degree and direction of tilt of the Fe−CN from the heme normal. The rhombic magnetic axes in S92A-metMbCN are rotated ∼10° in the opposite direction from the established ∼10° rotation for the axial His ring as expected. It is shown, moreover, that the pairwise α-, γ-meso vs β-, δ-meso-H hyperfine shift differences are well predicted by the change in the location of the rhombic magnetic axes. Carbon monoxide ligation rates experience minor but systematic perturbation for the S92A substitutions which confirms an influence (albeit very small) for axial His orientation on ligand affinity.

Myoglobin (Mb)[1] is a member of the large O_2 binding globin family that consists of a ∼150 residue chain arranged in eight helices (A−H) in a highly conserved globular fold with heme sandwiched between the E and F helices (*1*). The heme iron is linked to Nϵ of conserved His(F8) in the protein, and the remarkably varied ligation affinities and rates observed for natural genetic variants have been proposed to be modulated by distal interactions with, in particular, residues E7 (usually His, but also Gln in vertebrates), E11 (usually Val and Ile), and B10 (Leu in mammals and Phe or Tyr in some invertebrates) (*2*). The distal pocket in vertebrate Mbs and Hbs is thought to have evolved to strongly stabilize O_2 over CO binding, the latter of which binds more strongly to heme outside the protein matrix (*3*). There is general agreement that the stabilization of bound O_2 in globins is achieved in large part by a distal residue serving as a hydrogen bond donor to the bound ligand, as observed directly in the neutron diffraction study of MbO_2 (*4*). The factors that lead to destabilization of bound CO are more complex (*2*). However, the crystal structures of virtually all MbCO and HbCO find the Fe^{2+}−CO unit bent and/or tilted from the heme normal, and the general direction of tilt correlates with expected steric interaction with distal residue E11 whose orientation interferes with a linear FeCO unit normal to the heme (*5*, *6*). Alternatively, it has been proposed that FeCO bend/tilt is controlled from the proximal side by the axial His orientation (*7*, *8*).

The Fe^{3+}−CN unit in cyanomet Mb and Hb can serve as an extraordinarily sensitive probe of the structure of the heme pocket since Fe^{3+}−CN, like Fe^{2+}−O_2, is a H-bond acceptor (*9*−*15*), and like Fe−CO, prefers a linear orientation perpendicular to the heme (*16*). In cases where crystal structures of MbCO and metMbCN have been reported, the Fe^{2+}CO and Fe^{3+}CN units exhibit similar deformations (*15*−

† This research was supported by grants from the National Institutes of Health, HL16087 (G.N.L.), GM33775 (S.G.S.), and GM 31756 (S.G.S.).

* Author to whom correspondence should be addressed at University of California. Phone: (916) 752-0958. Fax: (916) 752−8995. E-mail: lamar@chem.ucdavis.edu.

‡ University of California.

§ University of Illinois.

[1] Abbreviations: Mb, myoglobin; metMb, met myoglobin; DSS, 2,2-dimethyl-2-silapentane-5-sulfonate; NOESY, two-dimensional nuclear Overhauser spectroscopy; TOCSY, two-dimensional total correlation spectroscopy; H97F-Mb, His97(FG3) → Phe Mb mutant; S92A-Mb, serine92(F7) → Ala Mb mutant; S92P-Mb, serine92(F7) → Phe Mb mutant.

S0006-2960(97)02829-8 CCC: $15.00
Published on Web 04/23/1998

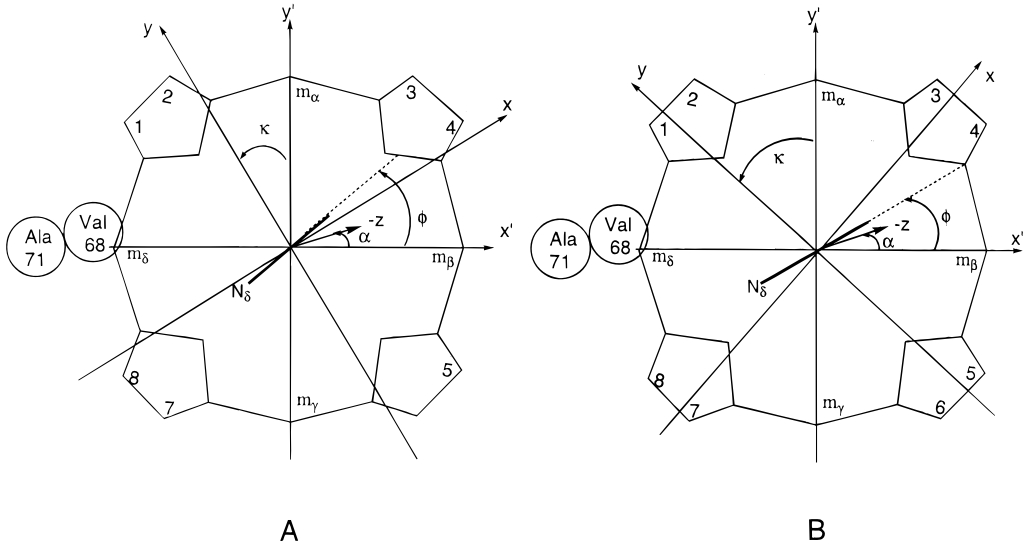

FIGURE 1: Schematic representation of the heme and axial His93(F8) imidazole plane and the position of the conserved distal Val68(E11) and Ala71(E11) in (A) sperm whale WT as observed in the crystal structure of MbCO (*5*), and (B) upon a ~10° clockwise rotation of the axial His93(F8) imidazole plane relative to a stationary heme as observed from S92A-Mb. The pseudosymmetry axes are x', y', and z', with z' normal to the heme. x, y, and z are the magnetic coordinate system in which the paramagnetic susceptibility tensor is diagonal, and are located by the Euler rotation $(x,y,z) = (x',y',z')\Gamma(\alpha,\beta,\gamma)$ where β is the tilt of the major or z-axis from the heme normal, α is the angle between that projection of the tilt of the z-axis on the heme plane and the x'-axis, and $\kappa \approx \alpha + \gamma$ locates the rhombic axes projected on the heme plane. The angle between the axial His93(F8) imidazole ring and the x'-axis is labeled ϕ.

18). While NMR of diamagnetic globin complexes can provide solution structural information similar to that obtained by X-ray crystallography, the detection of the labile proton in the H bond to O_2 is severely complicated by resolution, and there exist no solution spectral observables that relate to the Fe−CO tilt. In contrast, the large magnetic anisotropy of metMbCN induces significant dipolar shifts that provide exceptional resolution for residues close to the heme (*19*, *20*). Thus, resolution invariably allows the detection of the distal residue labile protons and direct demonstration of the H bond to the bound cyanide via detection of large isotope effects on the heme contact shifts (*21*, *22*).

The pattern of the heme pyrrole hyperfine shifts, dominated by the contact interaction, has been shown to directly reflect on the nature of the orbital ground state of the heme (*23*−*26*), which, in turn, is determined by the orientation of the axial His(F8) imidazole plane (with an angle ϕ with the x′ axis, as shown in Figure 1). Thus, alignment of the axial His with a N−Fe−N vector ($\phi = 45°$ in Figure 1), leads to large contact shifts solely for pyrrole A (1-CH_3) and C (5-CH_3), and negligible contact shifts for pyrrole B (3-CH_3) and pyrrole D (8-CH_3), while an alignment with meso-position ($\phi = 0$ or 90°) results in the same spin density on the four pyrroles with a minimum spread of the heme methyl contact shift. Thus, for a reference structure with $\phi = 40°$ (i.e., WT metMbCN), increase (decrease) in ϕ is expected to lead to an increased (decreased) spread of the heme methyl hyperfine shifts.

The observed dipolar shift, δ_{dip}, for nonligated residues is given by

$$\delta_{dip}(\text{calc}) = -\frac{1}{3N}\left[\Delta\chi_{ax}\frac{3\cos^2\theta' - 1}{R^3} + \frac{3}{2}\Delta\chi_{rh}\frac{\sin^2\theta'\cos 2\Omega'}{R^{-3}}\right]\Gamma(\alpha,\beta,\gamma) \quad (1)$$

where $\Delta\chi_{ax}$ and $\Delta\chi_{rh}$ are the axial and rhombic anisotropies of the diagonal paramagnetic susceptibility tensor χ, θ', Ω', R′ are the polar coordinates of a proton in an arbitrary iron-centered coordinate system, x', y', z', (R, θ', Ω') and $\Gamma(\alpha, \beta, \gamma)$ is the Euler rotation matrix that converts the arbitrary coordinate system, x', y', z' to the magnetic axes, x, y, z, (R, θ, Ω) in which χ is diagonal. The tilt of the major or z-axis from the heme normal is given by β, α is the direction of this tilt, defined as the angle between the projection of z on the x', y' plane and the x'-axis, and rhombic magnetic axes projected onto the heme plane is given by $\kappa \cong \alpha + \gamma$, as shown in Figure 1. The tilt of the major magnetic axis can be related to the tilt/bend of the Fe−CN unit. In the three cases where crystal structures (*7*, *17*, *27*) and NMR determined tilts of the magnetic axis are available (*10*, *13*, *14*, *22*), both the direction and qualitative degree of the tilt of the major axis agree well with the distortion of the Fe−CN unit in the crystal. In other cases where only MbCO diffraction data are available, the distortion of the major magnetic axis in metMbCN is in the same general direction as the off-axis distortions of the carbonyl in MbCO (*15*, *28*).

In this report, we investigate the influence of the proximal side mutations Ser92(F7) → Ala, Ser92(F7) → Pro, and His97(FG3) → Phe on the molecular, electronic and magnetic properties of the heme cavity of metMbCN complexes and on the CO ligation to the reduced Mb. The two residues are involved in hydrogen bonds that stabilize both the axial His imidazole ring and the heme in the cavity, as shown in Figure 2. The influence of those mutations will also be investigated by energy minimization. The orientation of the His(F8) imidazole, determined by the ring $N_\delta H$ serving as a H-bond donor to both the Ser side-chain Oγ and Leu89(F4) backbone (*5*), can be expected to be modulated upon abolishing the Ser Oγ H bond (*29*, *30*). Similarly, perturbation of the heme orientation can be expected by abolishing the 7-propionate to His97(FG3) side-chain salt bridge. Qualitative ^{1}H NMR studies have shown that a partial

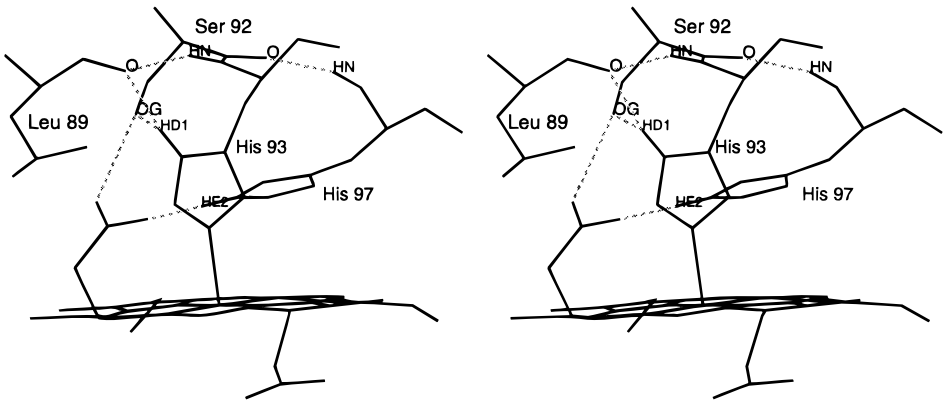

FIGURE 2: Stereoview of the hydrogen bond and salt-bridge network for the proximal side of sperm whale Mb.

collapse of the spread of the four heme methyl contact shifts occurs upon substituting Ser92(F7) → Ala in human metMbCN (*30*), which is consistent with rotation of the axial His relative to the heme, but does not uniquely distinguish whether the heme or axial His rotated. The perturbation by mutation of the relative orientations of the axial His and heme will be elaborated in terms of the relative influences on the orbital hole and rhombic axes.

MATERIALS AND METHODS

Mutagenesis and Protein Purification. All the mutants were constructed following procedures described by Springer and Sligar (*31*). The oligonucleotides were inserted into pMb122-9 plasmid, the plasmid containing the synthetic gene of SWMb with the amino acid at position 122 corrected to aspartic acid (*32*). Each mutation sequence was confirmed using the Sequenase double-stranded DNA sequencing reagents and protocol from United States Biochemicals (Cleveland, OH). The proteins were expressed in *Escherichia coli* and purified as described in Abadan et al. (*33*). The Mbs were oxidized by excess of potassium ferricyanide (2-fold) in an Amicon ultrafiltration cell and exchanged into ^2H_2O or 90% ^1H_2O:10% ^2H_2O, 100 mM KCl, and 20 mM phosphate to a concentration of ~4 mM. The mutant metMbH_2O complexes were initially prepared at pH 6.3, and pH titration was carried out in the range 6.3−9.8. The mutant metMbCN complexes were prepared by adding 20 mM KCN; pH titrations were carried out in the range 5.5−9.5. The pH was measured with a Beckman 3550 pH meter equipped with an Ingold microcombination electrode.

CO Binding Kinetics. Association and dissociation rate constants were measured for the binding of CO to the wild-type and mutant proteins according to the methods described by Rohlfs et al. (*34*) under pseudo-first-order conditions. All reactions were carried out at 20 °C in 0.1 M phosphate buffer, pH 7.4.

Energy Minimization. The WT sperm whale Mb crystal structure (pdb1mbc.ent) was used as a starting point. Using Quanta software (Molecular Simulations), residues 89, 92, and 97 were replaced by Ile, Ala, and Phe, respectively. Hydrogen atoms were added to the structure. The structures were then solvated and energy minimized using the CHARMM software package (Molecular Simulations) with principle structure file (PSF) to calculate energies. The poor nonbonded contacts were removed by 1000 steps of energy minimization using the steepest descent method followed by 500−1000 steps of energy minimization using the conjugate gradient method to refine the bond angles and distances and to allow the molecule to slowly converge to a local minimum.

NMR Spectra. All ^{1}H NMR spectra were collected at 25 °C on the GE Ω-500 spectrometer operating at 500 MHz. The chemical shifts were referenced to 2,2′-dimethyl-2-silapentane-5-sulfonate (DSS) through the water peak. The 1D experiments, nonselective T_1s, SUPERWEFT (*35*), and steady-state NOEs were carried out as described previously (*36*). The 1:1 experiment (*37*) was performed by using a modified pulse sequence composed of a standard 90° − *y*, τ, 90° − *y*, and an optional presaturation sequence pulse that allows comparison of two spectra with or without water suppression. The 1D data were processed on a Sun workstation using GE UNIX Ω software. All 2D experiments, MCOSY (*38*), NOESY (*39*), and TOCSY (*40*), were collected by using 2048 points for t_2, 512 blocks for t_1, typically 256 scans for each block, and a repetition rate ~2 s^{-1}. The spectral window was varied from 10 to 30 kHz, and the mixing times were 50 ms for NOESY and 30 ms for TOCSY. The 2D data were processed on the Silicon Graphics (SGI) workstation using the softare package Felix from Biosym (San Diego) and the structural simulations were carried out on SGI using the Biosym InsightII program.

Magnetic Axes Determination. The magnetic axes were determined as described in detail previously (*9*−*14*). Experimental dipolar shifts for structurally conserved portions of the heme pocket were used as input to search for the Euler rotation angles, α, β, γ, that transform the molecular pseudosymmetry coordinates [*x*′, *y*′, *z*′, or *r*, θ′, Ω′, (Figure 1)], readily obtained from crystal coordinates (*5*), into magnetic axes, *x*, *y*, *z*, by minimizing the following global error function:

$$F/n = \sum|\delta_{dip}(\text{obs}) - \delta_{dip}(\text{calc})|^2 \qquad (2)$$

$$\text{where} \quad \delta_{dip}(\text{obs}) = \delta_{DSS}(\text{obs}) - \delta_{DSS}(\text{dia}) \qquad (3)$$

and δ_{DSS}(obs) is the observed chemical shift referenced to DSS. δ_{DSS}(dia) is the shift in the isostructural diamagnetic MbCO complex (*41*, *42*) or calculated for protons whose δ_{DSS}(dia) are not available by using $\delta_{DSS}(\text{dia}) = \delta_{tetr} + \delta_{sec} + \delta_{rc}$, where δ_{tetr} is the shift in an unfolded tetra peptide (*43*, *44*), δ_{sec} is the shift of an amino acid proton typical for α-helices, β-strand, coils, etc. (*45*), and δ_{rc} is the heme-induced ring current shift (*46*). Minimizing the error function *F*/*n* in eq 2 was performed over three parameters, α, β, γ,

Table 1: CO Binding Data of Sperm Whale Myoglobin and Various Proximal Mutants[a]

protein	k_{on} (μM^{-1} s^{-1})	k_{off} (s^{-1})	K_a (μM^{-1})
sperm whale WT-Mb	0.50	0.018	28
sperm whale L89I-Mb	0.53	0.013	41
sperm whale S92A-Mb	0.62	0.015	41
sperm whale S92P-Mb	0.22	0.016	14
sperm whale H97F-Mb	0.61	0.014	44
human WT Mb[b]	1.02	0.02	51
human S92A-Mb[b]	1.34	0.01	134
pig WT Mb[c]	0.78	0.019	41
pig S92A-Mb[c]	1.10	0.019	57

[a] Sperm whale Mb kinetics were measured at pH 7.4 at 20 °C. [b] Human Mb kinetics taken from ref *30* were measured at pH 7.0 at 25 °C. [c] Pig Mb kinetics taken from ref *29* were measured at pH 7.0 at 20 °C.

using available $\Delta\chi_{ax}$ and $\Delta\chi_{rh}$ for WT metMbCN, as described in detail previously (*9*, *10*).

RESULTS

CO Binding Kinetics. All of the mutants, L89I, S92A, S92P, and H97F, were overexpressed as holoproteins in *E. coli* and are stable over periods of at least a week. The absorption spectra of the mutants are similar to the WT. An extra peak at 630 nm appeared in all of the proximal mutants. Initially, the extra peak was thought to be from the metMb species, which has a peak around 635 nm (*47*). However, when the samples were reduced and ligated with CO, the 630 nm peak shifted to 622 nm, indicating that the peak is not due to presence of met species. Myoglobin containing sulfheme has absorbance at 622 nm (*48*, *49*) and highly characteristic ^{1}H NMR (*50*) and EPR spectra (*51*). The absence of detectable sulfheme was confirmed by electron mass spectrometry and NMR and EPR spectroscopy. The 620 nm peak in the absorption spectra appears to be a manifestation of the proximal mutation, such that all the detected differences in mutants are due strictly to the residue substitution. The rates and equilibrium constants for CO binding to sperm whale L89I-Mb, S92A-Mb, and H97F-Mb, mutants are listed in Table 1 where they are compared to published data on sperm whale WT Mb and the WT and S92A-Mb mutants of pig (*29*) and human (*30*) Mbs.

Energy-Minimized Structures. The overall structure of the mutant Mbs was conserved, and the most significant differences localized at the mutation sites and the orientation of the axial His93(F8). The axial His imidazole ring was found rotated clockwise (viewed from the proximal side) by ∼2° for L89I-Mb and by ∼6° for S92A-Mb, and by counterclockwise rotation of ∼5° in H97F Mb compared to that in WT Mb.

Resonance Assignment. The 500 MHz ^{1}H NMR spectra of the four mutant metMbCN, together with that of WT (Figure 3B), are shown in Figure 3; the heme methyl assignments, as well as those for resolved resonances for His93(F8) and Ile99(FGs) are labeled. It is clear that, while there is a strong similarity among all of the spectra, there are small but systematic changes, with the low-field bias of the heme methyls decreasing monotonically for traces A − E in Figure 3; the low-field bias for H97F-metMbCN in trace A is larger than that for WT in trace B. The experimental protocol for effectively obtaining unambiguous assignments of the heme, axial His, and residues influenced by paramagnetic relaxation or shifts has been established (*52*) and tested on numerous mutants and natural genetic variants of metMbCNs and metHbCNs (*10*−*15*, *18*). Initial emphasis is on completely assigning the heme which exhibits resolved peaks for three methyls, a vinyl, and a propionate, followed by the axial His with characteristic large low-field ring $N_\delta H$ and $C_\beta H$ shifts. The remaining resolved resonances and unresolved resonances with strong to moderate temperature dependence of the shift arise from the target residue in the heme cavity that are needed to accurately define the magnetic axes, as discussed in detail elsewhere (*9*, *10*). The residue identities of such shifted and/or relaxed residues are unambiguously established by detection of the TOCSY spin connectivities diagnostic of that residue and the dipolar contact to other residues and the heme, as established for WT metMbCN. Any change in dipolar contacts among residues and between residues and the heme reflect on structural accommodation due to the point mutation. Since this procedure can be presented in detail elsewhere, we refer to and show representative data only for the most important of the present mutants, S92A-metMbCN, in Figure 4.

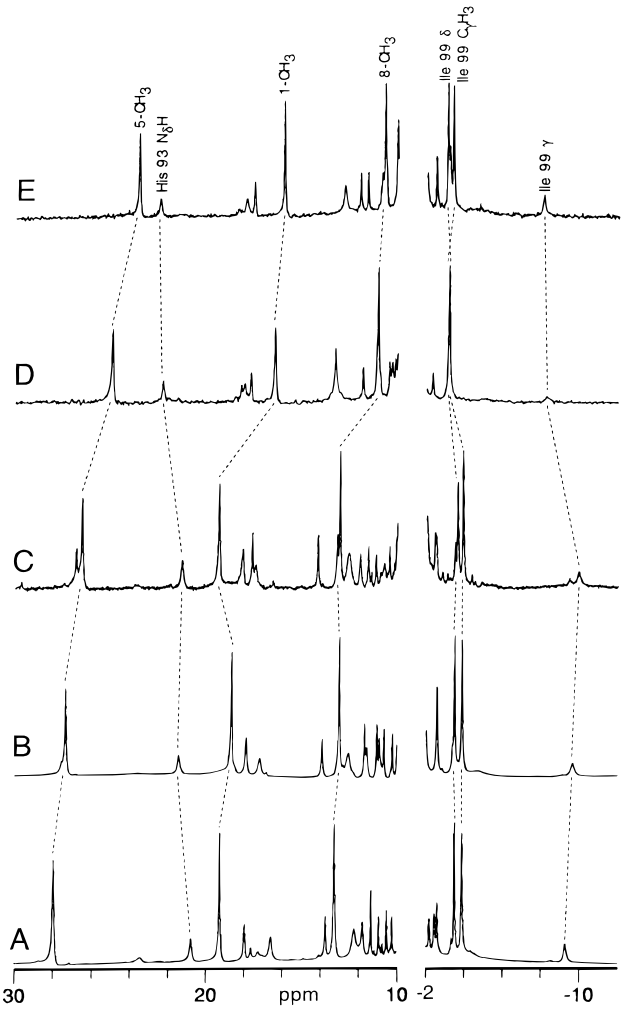

FIGURE 3: ^{1}H NMR spectra (500 MHz) of sperm whale (A) H97F-metMbCN, (B) WT metMbCN, (C) L89I-metMbCN, (D) S92A-metMbCN, and (E) S92P-metMbCN in H_2O and 0.2 M NaCl, pH 7, at 25 °C. The resolved signal for the heme and Ile99(FG5) is labeled.

Heme and Axial His. The three low-field methyls exhibit no TOCSY/COSY connectivity, but a weak NOESY cross-peak between two locate the 1-CH_3 and 8-CH_3 pair. NOESY

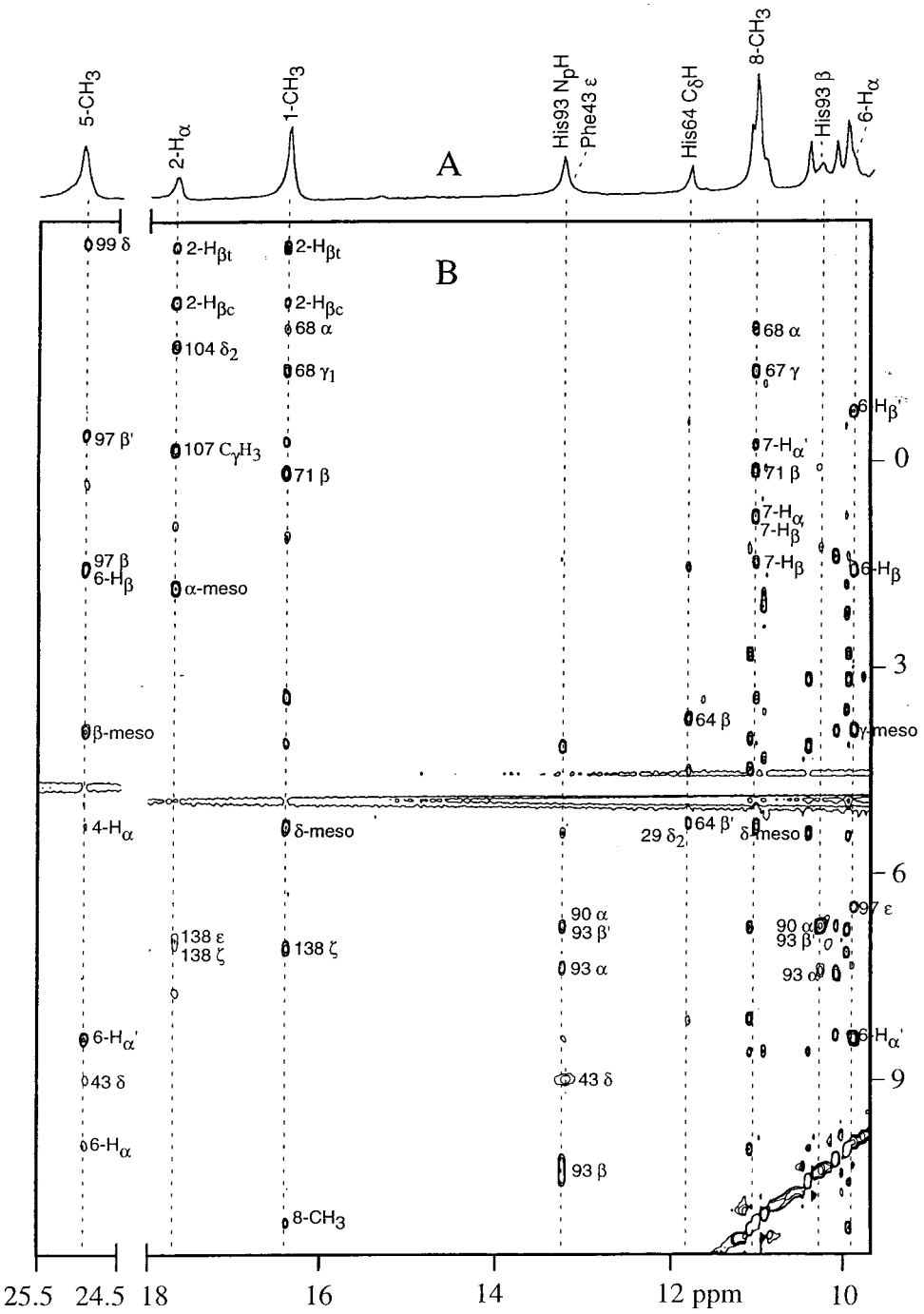

FIGURE 4: (A) The resolved downfield portions of the 500 MHz [1]H NMR spectrum of S92A-metMbCN in H_2O, pH 7, at 25 °C. (B) Portions of the NOESY spectrum of S92A-metMbCN with 100 ms mixing time in H_2O, pH 7, at 25 °C, showing the key intraheme and heme-residue contacts.

connectivity (representative data shown in Figure 4) for these 1-CH_3 and 8-CH_3, one each to a TOCSY detected vinyl and propionate spin systems, identifies 1-CH_3, 8-CH_3, 2-vinyl, and 7-propionate group. The third methyl also exhibits NOESY cross-peaks to a propionate with some resolved peaks that must arise from 5-CH_3 and 6-propionate. A second, nonresolved TOCSY-detected vinyl group exhibits NOESY cross-peaks to a methyl candidate that must arise from the remaining 4-vinyl and 3-CH_3. The detection of NOESY cross-peaks from methyl, vinyl, and/or propionate to a common strongly relaxed proton with Curie intercepts in the downfield region locates the four meso-Hs (Table 2).

A remaining low-field resolved proton at 11 ppm exhibits TOCSY/NOESY cross-peaks to both geminal and vicinal protons (the latter of which also exhibits a COSY peak to a labile proton), as well as a NOESY cross-peak to a strongly relaxed ($T_1 \approx 25$ ms) labile proton at 22 ppm characteristic of the axial His ring $N_\delta H$, assigning the $C_\beta H_2 C_\alpha H$ fragment of His93(F8). Two very broad (400 Hz) and strongly relaxed ($T_1 \approx 3$ ms) protons near ~20 and −4 ppm must originate from the His(F8) ring $C_\epsilon H$, $C_\delta H$ (*36*). The chemical shifts of the heme and axial His of S92A-metMbCN, as well as for the other two mutants, are listed in Tables 2 and 3 where they can be compared to similar data for WT metMbCN. It

Table 2: Heme Proton Chemical Shifts of Sperm Whale Proximal Mutant MetMbCN Complexes[a]

proton	L89I	S92A	S92P	H97F	WT[b]
1-CH_3	19.26	16.39	15.95	19.28	18.62
3-CH_3	4.50	4.26	4.31	4.01	4.76
5-CH_3	26.45	24.95	23.58	27.84	27.03
8-CH_3	12.99	11.03	10.70	13.19	12.88
2-H_α	18.02	17.65	17.52	17.90	17.75
2-$H_{\beta c}$	−1.61	−2.34	−2.49	−1.64	−1.73
2-$H_{\beta t}$	−2.51	−3.14	−3.18	−2.46	−2.55
4-H_α	5.51	5.28	5.37	5.33	5.50
4-$H_{\beta c}$	−1.97	−0.97	−0.85	−2.18	−1.95
4-$H_{\beta t}$	−0.74	0.03	0.20	−0.92	−0.77
6-H_α	9.21	9.90	10.84	9.44	9.18
6-$H_{\alpha'}$	7.12	8.38	7.93	6.92	7.35
6-H_β	1.68	1.59	1.00	1.54	1.67
6-$H_{\beta'}$	−0.43	−0.75	−1.38	−0.48	−0.48
7-H_α	1.08	0.77	1.28	−0.55	1.13
7-$H_{\alpha'}$	−0.17	−0.25	−0.38	−1.70	−0.45
7-H_β	1.50	1.44	2.04	1.98	1.55
7-H_β'	0.70	0.77	0.26	0.75	0.78
α-*meso*-H	4.61	1.81	1.92	4.94	4.40
β-*meso*-H	1.68	3.92	4.21	1.16	2.09
γ-*meso*-H	5.14	3.89	3.82	6.25	5.98
δ-*meso*-H	5.12	5.28	5.16	4.30	4.09
$\Delta\delta_{meso}$(obs)[c]	1.48	−1.75	−1.82	2.97	2.1

[a] In parts per million, from DSS, at 25 °C and pH 7. [b] Data from ref *36*. [c] Defined by eq 4.

is observed that the spread of the four heme methyls is slightly larger in H97F-metMbCN than WT metMbCN, which in turn, is larger than that for S92A-metMbCN and S92P-metMbCN. The prevailing qualitative model (*23*, *26*, *52*) for interpreting these differences in contact shifts indicates that the axial His93(F8) imidazole plane relative to the heme is rotated counterclockwise (viewed from the proximal side) in H97F-metMbCN and clockwise in S92A- and S92P-metMbCN, relative to that in WT metMbCN.

Nonligated Residues. The resolved and strongly relaxed ($T_1 \approx 20$ ms) low-field peak at 16 ppm exhibits a NOE to a partially resolved and moderately relaxed two proton signal at 12 ppm, which, in turn, exhibits a TOCSY peak to 9 ppm. The intercepts in the aromatic window in a Curie plot, together with characteristic NOESY peak to the heme 5-CH_3 (Figure 4), identify the complete Phe43(CD1) ring. A resolved labile proton peak near 22 ppm (which exhibits saturation transfer from bulk water), exhibits an NOE to the resolved single proton peak characteristic of the His64(E7) $N_\epsilon H$ and $C_\delta Hs$. The moderated relaxed upfield peak at −10 ppm is part of a complete TOCSY connectivity characteristic of Ile with NOESY cross-peaks to 5-CH_3, 4-vinyl, and 3-CH_3, as expected solely for Ile99(FG5). The remaining upfield resolved single proton exhibits TOCSY connectivity of a Val and the characteristic $C_\alpha H$ NOE to 1-CH_3 and 8-CH_3 diagnostic for Val68(E11). The conserved complete Ala71-(E14), Thr67(E10), Ala90(F5), the ring of Phe138(H15), the isopropyl fragment of Leu104(G5), the ethyl fragment of the Ile107(G8), and isopropyl fragment of Leu29(B10) were identified by the characteristic TOCSY cross-peak pattern and the expected NOESY cross-peak to the 1-CH_3, 8-CH_3, 8-CH_3 and 7H_α, His93(F8) $C_\beta Hs$, 2-vinyl, 3-CH_3 and 2H_β, and 3-CH_3-2H_α and His64(E7) $C_\delta H$, respectively (not shown; see Supporting Information).

In all mutants except H97F-metMbCN, His97(FG3) was assigned by the expected NOE from its TOCSY connectivity

Table 3: Chemical Shift for Heme Pocket Residues in Sperm Whale Proximal Mutant MetMbCN Complexes[a,b]

residue	proton	L89I	S92A	S92P	H97F	WT[c]
Leu29(B10)	$C_\gamma H$	3.96	3.87	3.55	3.96	3.90
	$C_{\delta 1}H_3$	3.68	3.72	4.08	3.71	3.81
	$C_{\delta 2}H_3$	5.40	5.24	5.27	5.40	5.53
Phe43(CD1)	$C_\delta Hs$	8.69	8.97	8.77	8.56	8.70
	$C_\epsilon Hs$	12.52	13.20	12.79	12.29	12.58
	$C_\xi H$	17.43	18.17	17.91	16.71	17.27
His64(E7)	$C_\beta H$	3.68	3.72	3.69	3.68	3.81
	$C_\beta H'$	4.35	5.24	4.37	4.30	4.41
	$C_\delta H$	11.52	11.79	11.59	11.37	11.74
	$N_\epsilon H$	23.8	24.5	24.1	23.6	23.7
Thr67(E10)	$C_\alpha H$	2.47	2.61	2.63	2.47	2.50
	$C_\beta H$	2.65	2.85	2.78	2.63	2.68
	$C_\gamma H_3$	−1.61	−1.34	−1.31	−1.56	−1.51
Val68(E11)	$C_\alpha H$	−2.44	−1.95	−1.64	−2.59	−2.55
	$C_\beta H$	1.24	1.45	1.61	1.26	1.47
	$C_{\gamma 1}H_3$	−1.15	−1.34	−0.88	−1.28	−1.02
	$C_{\gamma 2}H_3$	−0.20	−0.57	−0.27	−1.02	−0.89
Ala71(E14)	$C_\alpha H$	3.47	3.60	3.61	3.47	3.48
	$C_\beta H_3$	−0.16	0.11	0.18	−0.18	−0.12
Leu/Ile89(F4)	$C_\alpha H$	8.86	8.58	8.58	8.37	8.71
Ala90(F5)	$C_\alpha H$	6.41	6.69	6.47	6.39	6.50
	$C_\beta H_3$	2.63	2.77	2.44	2.65	2.63
His93(F8)	NH	14.15	13.25	11.96	13.75	13.90
	$C_\alpha H$	7.34	7.45	7.06	7.56	7.51
	$C_\beta H$	11.91	10.30	10.00	11.80	11.68
	$C_\beta H'$	6.20	6.76	7.59	6.28	6.43
	$C_\delta H$	−5.4	−5.1	−4.5	−4.3	−4.7
	$C_\epsilon H$	19.0	21.7	21.6	17.4	19.2
	$N_\delta H$	21.30	22.28	22.47	20.80	21.11
His/Phe97(FG3)	$C_\alpha H$	3.60	3.64	3.05	3.86	
	$C_\beta H$	1.16	1.48	1.52	1.14	1.32
	$C_\beta H'$	−0.48	−0.40	0.22	0.29	−0.48
	$C_\delta H$	10.75	11.03	10.70	7.61	11.07
	$C_\epsilon H$	6.79	6.47	6.79	8.0	6.83
	$C_\xi H$				6.75	
Ile99(FG5)	$C_\alpha H$	2.29	2.57	2.50	2.29	2.34
	$C_\beta H$	−0.25	0.07	0.11	−0.02	−0.12
	$C_\gamma H_3$	−3.62	−3.18	−3.36	−3.49	−3.46
	$C_\gamma H$	−9.97	−8.30	−8.10	−9.25	−9.60
	$C_\gamma H'$	−2.03	−1.60	−1.35	−1.64	−1.91
	$C_\delta H_3$	−3.93	−3.18	−3.06	−3.88	−3.83
Leu104(G5)	$C_\gamma H$	0.01	−0.04	−0.18	0.11	0.07
	$C_{\delta 1}H_3$	0.42	0.35	0.33	0.87	n/a
	$C_{\delta 2}H_3$	−1.70	−1.71	−1.95	−1.38	−1.49
Ile107(G8)	$C_\gamma H_3$	0.36	−0.19	−0.10	0.49	0.37
Phe138(H15)	$C_\delta Hs$	7.05	7.06	6.88	7.05	7.02
	$C_\epsilon Hs$	6.92	6.90	6.78	6.94	6.94
	$C_\xi H$	7.05	7.06	6.88	7.02	7.00

[a] In parts per million from DSS, at 25 °C and pH 7. [b] The $C_\epsilon Hs$, $C_\delta Hs$ shifts, in parts per million, for Tyr146(H23) are 7.18, 7.46 (L89I); 7.18, 7.46 (S92A); 7.15, 7.43 (S92P)); 7.15, 7.38 (H97F). [c] Data taken from ref *36*.

detected $C_\beta H_2 - C_\alpha H$ fragment to the 5-CH_3, the strongly relaxed ($T_1 \approx 20$ ms) ring $C_\delta H$ contact to His93(F8) $C_\alpha H$, and the contact of $C_\epsilon H$ to 6-H_αs. In the H97F-metMbCN, the Phe97(FG3) $C_\alpha H - C_\beta H_2$ fragment was detected as in WT and the other mutants; a TOCSY-detected three-spin system with chemical shift in the aromatic window identifies the ring (with the expected $C_\epsilon H$ contact to 6H_α). The $C_\alpha Hs$ of Leu89(F4) in all mutants and of Ile89(F4) in L89I-metMbCN were identified by their characteristic strong low-field shift and NOESY cross-peaks to His93(F8) $C_\beta H$ (not shown). The chemical shifts for the residues of interest are listed in Table 3 where they can be compared with the shift for WT metMbCN.

The assigned distal residues exhibit in detail the same pattern of NOESY cross-peaks and paramagnetic relaxivity

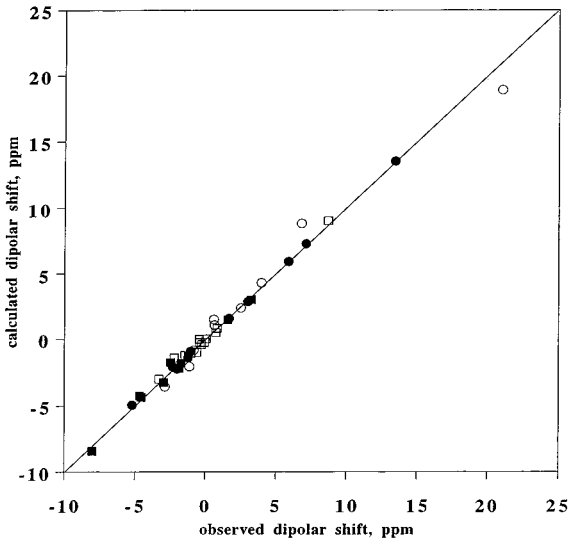

FIGURE 5: Plot of δ_{dip}(obs) vs δ_{dip}(calc) for S92A-metMbCN for the optimized magnetic axes $\alpha = 10°$, $\beta = 16°$, and $\gamma = 40°$, with $\Delta\chi_{ax} = 2.02 \times 10^{-9}$ m^3/mol and $\Delta\chi_{rh} = -0.453 \times 10^{-9}$ m^3/mol. The proximal and distal side input data are shown as solid circles and squares, respectively, and other noninput assigned distal and proximal residue signals are shown as open circles and squares, respectively.

observed in WT metMbCN (*10*, *36*), which can be taken as direct evidence for insignificant structural accommodation of the distal pocket to the proximal mutation. The assigned proximal residues in each case are the same as those identified in WT and distal mutant metMbCNs (*10*−*15*), in each case with essentially unchanged paramagnetic relaxation and dipolar contact to the heme and each other except for the mutated residues. Because Leu89(F4) in WT Mb exhibits a variety of conformations even in WT (*9*) likely because of the proximity to the "Xenon" hole (*54*), assignment and analysis of the remainder of Ile89(F4) in L89I-metMbCN was not pursued. Neither the S92A- nor, more surprisingly, the S92P-metMbCN mutant exhibited detectable perturbations of the dipolar contact among the assigned conserved residues or to the heme.

Determination of Magnetic Axes. The magnetic axes were obtained for each mutant using the proton dipolar shifts only for conserved residues [except for $C_\alpha H$ of Ile89(F4)] as input, as reported previously for WT metMbCN (*10*). These consisted of 20 protons, 10 from residues on the proximal and 10 from the residues on the distal side. The calculations were performed in a three-parameter search for α, β, γ using the magnetic anisotropies determined for WT metMbCN (as shown insignificantly changed in all distal mutants studies), $\Delta\chi_{ax} = 2.02 \times 10^{-9}$ m^3/mol and $\Delta\chi_{rh} = -0.453 \times 10^{-9}$ m^3/mol. The fits provide an excellent correlation between observed and calculated dipolar shifts, as shown in Figure 5. The determination of $\Gamma(\alpha,\beta,\gamma)$, moreover, was performed using either only the 10 proximal protons or only the 10 distal protons, as well as using both the 10 distal and 10 proximal protons, with a summary of the results given in Table 4. Inspection of Table 4 reveals that, in each case, the angles varied with the choice of input data as $\beta < 1°$, $\alpha < 10°$, and $\kappa < 10°$. Analysis of the influence of a variety of input data on $\Gamma(\alpha, \beta, \gamma)$ for WT metMbCN had indicated that the Euler angles have uncertainties of ± 1 in β, $\pm 10°$ in α, and $\pm 10°$ in κ (*10*), such that it can be concluded (except for S92P metMbCN; see below) that the degree of tilt (β) and direction of tilt (α) are essentially unchanged for the proximal mutants when compared to similar data for WT metMbCN.

Table 4: Orientation of the Magnetic Axes for Sperm Whale Proximal Mutants MetMbCN Complexes[a]

		orientation angles[b]			
protein	input[c]	α	β	$\kappa = \alpha + \gamma$	F/n (ppm^2)
L89I	t20	20°	16°	30°	0.07
	d10	20°	15°	40°	0.04
	p10	20°	16°	30°	0.07
S92A	t20	10°	16°	50°	0.09
	d10	10°	16°	50°	0.04
	p10	0°	17°	50°	0.11
S92P	t20	10°	15°	50°	0.09
	d10	20°	15°	50°	0.05
	p10	0°	17°	50°	0.10
H97F	t20	20°	15°	30°	0.05
	d10	20°	15°	30°	0.03
	p10	20°	14°	30°	0.08
WT[d]	t20	20°	15°	30°	0.05
	d10	20°	15°	40°	0.03
	p10	20°	15°	30°	0.06

[a] The magnetic axes were calculated by using three-parameter least-squares searches at 25 °C with $\Delta\chi_{ax} = 2.02 \times 10^{-9}$ m^3/mol and $\Delta\chi_{rh} = -0.453 \times 10^{-9}$ m^3/mol, taken from WT metMbCN (*11*). [b] The angle definitions have been shown in Figure 1. The error range is $\pm 1°$ for β, $\pm 10°$ for α and $\pm 10°$ for κ. [c] The total 20 protons (abbreviated as t20) are half from distal residues (d10): Leu B10 $C_\gamma H$ and $C_{\delta 2}H_3$, Phe CD1 C_δHs, C_ϵHs and C_ζH, Thr E10 $C_\alpha H$, Val E11 $C_\alpha H$, Ala E14 $C_\alpha H$ and $C_\beta H_3$ and Ile G8 $C_\gamma H_3$. Half from proximal residues (p10): Ala F5 $C_\alpha H$ and $C_\beta H_3$, Ile FG5 $C_\alpha H$, $C_\beta H$, $C_\gamma H$, $C_\gamma H'$, $C_\gamma H_3$ and $C_\delta H_3$ and Leu G5 $C_\gamma H$ and $C_{\delta 2}H_3$. [d] For comparison, the magnetic axes of WT metMbCN were re-calculated by using the same input as those for the mutants.

The rhombic axes (κ) for L89I-metMbCN and H97F-metMbCN are also essentially the same as those of WT metMbCN (Table 4). However, κ for S92A- and S92P-metMbCN is larger, generally by 20°, than for WT and other distal mutant metMbCN complexes (*10*−*15*). While the 20° difference is not clearly outside the experimental uncertainty of κ, the consistent increase in κ in the two position 92 mutants over WT metMBCN strongly favors a counterclockwise rotation of the rhombic axes (Figure 1) in the two mutants. The Phe97(FG3) ring in H97F-metMbCN was found to exhibit a good correlation between δ_{dip}(obs) and δ_{dip}(calc) when the ring center was translated relative to the imidazole by 0.4 Å over the heme plane and away from the iron. The magnitude and direction of the movement is consistent with the larger size of the phenyl ring.

Distinction between Axial His and Heme Rotation. Assuming that a small ($\leq 10°$) rotation of either heme or axial ligand is a completely local phenomenon and does not perturb the remaining structure of the heme cavity, inspection of the molecular structure of WT Mb reveals that such rotation can be monitored by alteration in the dipolar contacts between the rotating entity (heme or axial His) and backbone protons on the E and F helices. Thus, a clockwise rotation of the His93(F8) imidazole plane by 10° (Figure 1) decreases both the intraresidue His93(F8) $N_\delta H - C_\beta H$ and interresidue His93(F8) $N_\delta H$ to Leu89(F4) $C_\alpha H$ distances by 3−4%, leading to the expectation of increased NOEs by ~20% ($\propto r_{ij}^{-6}$) from the His93(F8) $N_\delta H$ to these two protons. The quantitation of the rotation of the heme about the axial bond

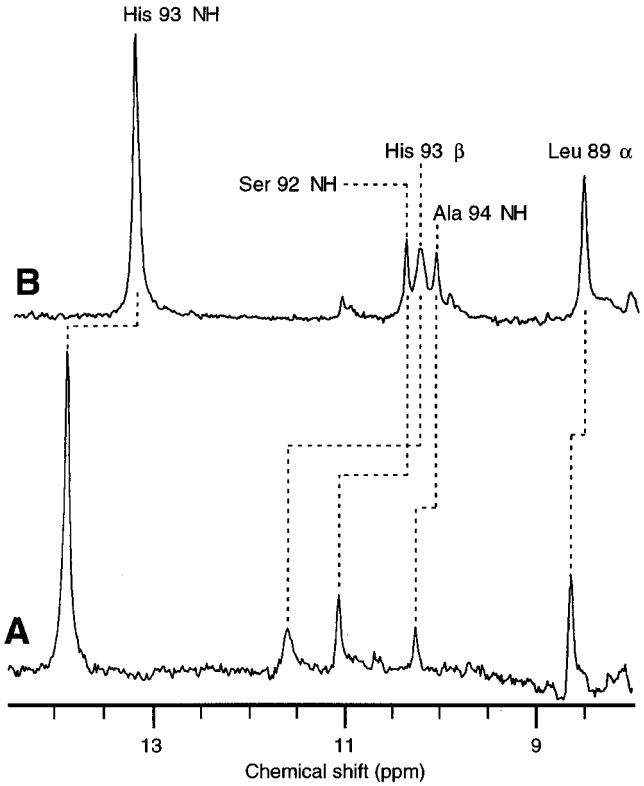

FIGURE 6: Steady-state NOE difference spectra upon saturating the His93(F8) $N_\delta H$ signal in (A) WT metMbCN and (B) S92A-metMbCN in H_2O, pH 7.0, at 25 °C, showing the different peak intensities of HisF8(93) N_pH and $C_\beta H$, as well as the Leu89(F4) $C_\alpha H$. The intensity of the saturated $N_\delta H$ signal is identical for the two traces.

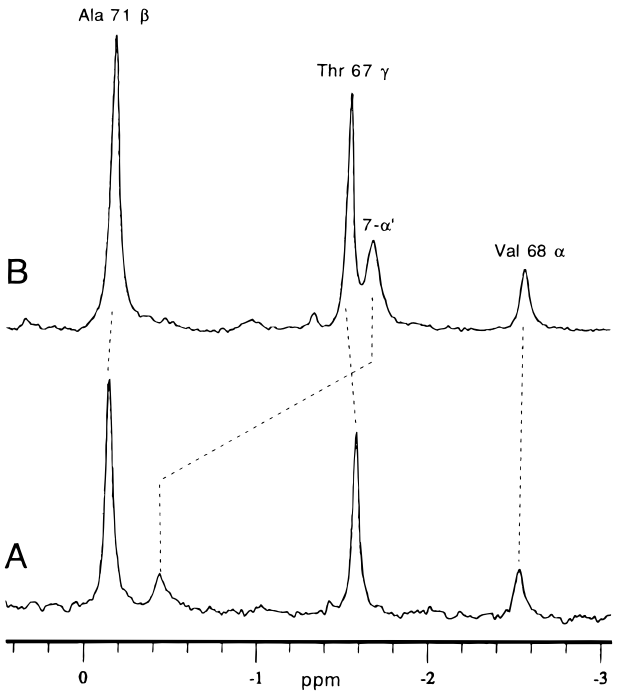

FIGURE 7: Steady-state NOE difference spectra upon saturating the heme 8-CH_3 signal in (A) WT metMbCN and (B) H97F-metMbCN in ^2H_2O, pH 7.0 at 25 °C illustrating the differences in the magnitude of the NOEs to $C_\alpha H$ of Val68(E11) and $C_\beta H_3$ of Ala71(E14). The intensity of the saturated 8-CH_3 signal is identical in the two traces.

is conveniently achieved by monitoring the distance from the 8-CH_3 to the $C_\alpha H$ of Val68(E11) or $C_\beta H_3$ of Ala71(E14). A ~3° clockwise[2] rotation of the heme as viewed from the proximal side would decrease each of these distances by ~4%, leading to increased steady-state NOEs of ~25%.

For S92A-metMbCN, the steady-state NOEs upon saturating 8-CH_3 to Ala71(E14) $C_\beta H_3$ and Val68(E11) $C_\alpha H$ are essentially the same as for WT metMbCN (*11*), indicating an unchanged position of the heme relative to the protein matrix (not shown). The steady-state NOEs resulting from saturating the His(F8) $N_\delta H$ signal in WT metMbCN and S92A-metMbCN are shown in Figure 6; the degree of saturation of the His(F8) $N_\delta H$ is identical in the two traces. It is observed that the NOEs to His(F8) $C_\beta H$ and Leu89(F4) $C_\alpha H$ increase by 15−30%, while that to His93(F8) N_pH decreased. These changes are in semiquantitative agreement with the ~10° clockwise rotation of the imidazole of His F8 relative to the stationery heme in S92A-metMbCN (Figure 1). For H97F-metMbCN, the steady-state NOEs to the His-(93) N_pH, $C_\beta H$, and Leu89(F4) $C_\alpha H$ upon saturating His93-(F8) $N_\delta H$ are essentially the same as for WT metMbCN (not shown). On the other hand, the steady-state NOEs from the 8-CH_3 to Ala71(E14) $C_\beta H_3$ and Val68(E11) $C_\alpha H$ are ~25% larger[2] (Figure 7B) than in WT (Figure 7A), which is consistent with a 3° clockwise rotation of the heme relative to the stationary His93(F8) and E helix.

Influence of pH on Proximal Mutant metMbCN. A pH titration of WT-metMbCN revealed significant heme shift changes (up to 1.5 ppm) for the heme 5-CH_3 at low pH that reflect a pK ~ 5.2 that has been attributed to the breaking of the 7-propionate-His97(FG3) hydrogen bond (*55*); in particular, the Ile99(FG5) $C_\gamma H$ signal experienced an 0.8 ppm shift change with pH, directly documenting the link between the 7-propionate and FG corner. A similar pH titration for H97F-metMbCN reveals much weaker heme chemical shift changes (≤0.2 ppm) at low pH that similarly reflect a pK ~5, with minimal pH influence on Ile99(FG5) $C_\gamma H$ and 5-CH_3 (not shown). The significant reduced amplitude of the pH effect is consistent with the absence of a hydrogen bond to the 7-propionate in the mutant.

The axial His93(F8) ring $N_\delta H$ exhibited intensity decreases of ~35 ± 10% (saturation factor $F = 0.65 \pm 0.10$) when the water signal is saturated at strongly alkaline, but not neutral, pH (not shown; see Supporting Information), indicating that the proton exchanges with bulk water. Together with the His93(F8) $N_\delta H$ $T_1 \approx 25$ ms at pH 8.0 (where there is no saturation transfer at lower pH), the His(F8) $N_\delta H$ exchange rates with water, k, calculated from $F = (1 + kT_1)^{-1}$ (*56*), are similar at 20 ± 5 s^{-1} for WT and all proximal mutant metMbCN complexes at 25 °C and pH 8.6.

metMbH$_2$O Spectra. The low-field portions of the 500 ^1H MHz NMR spectra of the high-spin metMbH$_2$O at pH 6 (Figure 8) reveal a total of 10 relatively narrow (~250 Hz) signals, four methyls and six single proton peaks between 25 and 100 ppm, as well as a very broad composite near 40 ppm (as shown in Figure 8A), for which complete assignments have been reported for WT (*57*). The chemical shifts

[2] The 3° clockwise rotation would similarly increase the distance between heme 1-CH_3 and the Val68(E11) $C_\alpha H$ and Ala71(E14) $C_\beta H_3$ leading to a similar decreased NOE. While a clear decrease in the NOE to these two signals is observed upon saturating the 1-CH_3, the magnitude of the NOE cannot be quantitated in the mutants because the 1-CH_3 overlaps the $2H_\alpha$ signal at all temperatures, making it difficult to quantitate the degree of 1-CH_3 saturation.

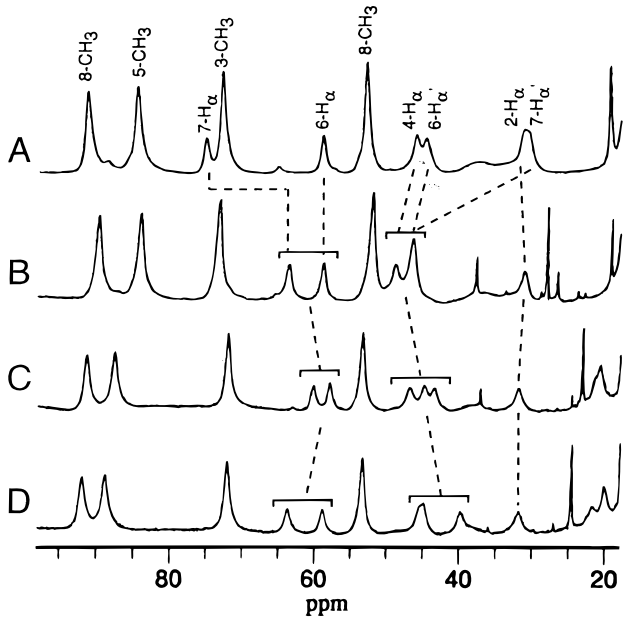

FIGURE 8: [1]H NMR spectra (500 MHz) for the met−aquo complexes of (A) sperm whale wild-type (with assignments reported previously); (B) S92A-Mb; (C) S92P-Mb; and (D) H97F-Mb in ^2H_2O, pH 6.3, 50 mM in NaCl, 25 °C.

for the heme methyls are strongly conserved among the mutants and WT. The most notable difference between the proximal mutants and WT [1]H NMR spectra are the chemical shifts of the 7-propionate H_α signals at 75 and 25 ppm in WT, which are much closer together (∼60 and 50 ppm) in all of the mutants. The large difference in the $7H_\alpha$ primarily contact shifts in WT metMbH_2O was previously shown (*57*) to be consistent with the orientation of the 7-$C_\alpha H_2$ needed to maintain a salt bridge to the His97(FG3) ring (*58*). Mutation to either His97(FG3) or Ser92(F7) results in very similar 7-propionate orientations which are different from that in WT. The $7H_\alpha$ contact shifts are consistent with a more extended orientation of the 7-propionate group that would be unable to hydrogen bond to either His97(FG3) or Ser92(F7).

The nearly identical heme methyl contact shifts of the proximal mutants and WT metMb, including the low-field obvious meso-H peak at 40 ppm, reveal six coordinate species with a ligated water in each case. Increasing the pH resulted in each case in broadening of resonances with subsequent loss of intensity and the appearance of new peaks in the 10−50 ppm window that are very similar to those of WT metMbOH (not shown; see Supporting Information). The similar influence of pH on line widths and chemical shifts indicates that the proximal mutations considered here do not significantly perturb either the thermodynamics or dynamics of the acid → alkaline transition of metMb (*59*).

DISCUSSION

Heme Cavity Structure of Mutants. The conserved residues in the various mutants exhibited essentially the same pattern of paramagnetic-induced relaxivity and dipolar contacts with the heme and with each other as observed in WT metMbCN (*10*, *36*). This is particularly the case for the distal pocket. On the proximal side, the effect of the L89I mutation was minimal, as can be expected based on the residue lining an existent "vacancy" (*54*, *58*). For the S92A mutant, even the proximal heme contacts are conserved, with the only clearly detectable change that of the ∼10° clockwise rotation of the His93(F8) imidazole ring described above. The small change in His ring orientation is readily accommodated by the pocket without any van der Waals surface violations and is completely consistent with the results of the energy minimization studies. It is assumed that a similar reorientation of His93(F8) occurs in the less extensively investigated S92P-metMbCN. The position of the ring of Phe97(FG3) in H97F-metMbCN, while centered ∼0.4 Å further from the iron on the heme face, still makes ideal van der Waals contact with the heme, His93(F8), Lys96(FG2), and Ile99(FG5).

The reorientation of the axial His ring by 10° upon replacing Ser92(F7) is so as to place the $N_\delta H$ in optimal position to make a stronger bond to the Leu89(F4) carbonyl. The essentially unaltered exchange rate of the His93(F8) ring $N_\delta H$ with bulk water in the proximal mutants, when compared with WT metMbCN (*56*), attests to the conserved strength of the hydrogen bond, albeit with only (but optimally oriented) the Leu89(F4) carbonyl. The influence of the S92A mutation on the [1]H NMR spectra of human (*30*) and sperm whale metMbCN are very similar, with the change in the 5-CH_3 shift slightly larger (2.7 ppm) in human than sperm whale (2.4 ppm) mutants. These results indicate that the axial His in human S92A-metMbCN is similarly rotated by at least 10°.

The very similar 7-H_αs contact shifts in H97F-, S92A-, and S92P-metMbH_2O, when compared with the disparate $7H_\alpha$ shifts in WT metMbH_2O (Figure 8), reflect an extended 7-propionate orientation in each of these mutants. The essentially identical effect on the $7H_\alpha$ contact shifts in the three proximal mutants indicates that the 7-propionate hydrogen bonds to the His97(FG3) ring and Ser92(F7) O_γ are severed when either of these two residues are substituted by nonpolar groups. The absence of any direct link between the 7-propionate and the FG corner in H97-metMbCN is verified by the minimal effect of pH on the Ile99(FG5) chemical shifts, as was observed for low pH in WT metMbCN. The crystal structure of the pig S92L-Mb mutant revealed a disordered 7-propionate with a severed link to His92(FG3) (*29*). The change in NOEs between 8-CH_3 and Val68(E11) $C_\alpha H$ or Ala71(E14) $C_\beta H_3$ indicate a very slight (∼3°) clockwise rotation[2] of the heme relative to the static His93(F8) ring in H97F-metMbCN when compared to WT. The 7-propionate−protein interaction, while likely stabilizing the heme binding in general, does not exert a strong control over the heme orientation. The direction of the heme rotation is the same, but with smaller magnitude, than predicted for energy minimization.

Structure−Function Correlations. The potential role of axial His orientation on ligation rate have been recognized (*29*, *30*, *60*, *61*), but studies to date (*29*, *30*, *33*, *62*) indicate that the effects are more subtle than distal influences, and their complete understanding will require additional data. Our present [1]H NMR data substantiate a ∼10° rotation of the axial His, which results in a ∼1.5-fold increase in the CO affinity due to a small increase in k_{on} and a small decrease of k_{off} (Table 1). A faster k_{on} and slower k_{off} are consistent with less His $C_\epsilon H$, $C_\delta H$ steric interaction with the pyrrole N when the axial His is rotated 10° from that in WT Mb. While the changes in rates are small, they reflect the same pattern

as observed for human (*30*) and pig (*29*) from WT and S92A-Mb mutants for which a similar axial His rotation can be inferred from the NMR at least for human S92A metMbCN. However, it should be noted that the CO rates are changed similarly in the S92A- and H97F-Mb mutants, despite rotation of the axial His in the opposite direction. In the latter case, the effect of the small rotation of the His plane may be secondary to more direct electronic effects due to the position 97 aromatic ring on the heme not directly manifest in NMR parameters. The minimal effect of the proximal mutations on the iron ligand reactivity is further supported by unchanged p*K* and rate for the acid → alkaline transition relative to that of WT.

The Major Magnetic Axis. It is noted that the use of either only proximal or only distal residue dipolar shifts resulted in the same magnetic axes for each of the mutant metMbCN, and, moreover, the magnitude of the tilt of the major magnetic axes from the heme normal, $\beta = 15° \pm 1°$, and direction of tilt, $\alpha = 10 \pm 10°$, are the same as in WT metMbCN (Table 4) (*9*, *10*). Even the ~10° reorientation of His93(F8) in S92A-metMbCN (and likely S92P-metMbCN) fails to produce a significant change in either α or β. Inasmuch as both magnitude and direction of tilt of the major magnetic axis could be manipulated at will with distal residue mutations (*11*−*15*), *the present results provide strong support that the major magnetic axis is controlled by distal and not proximal interactions*. In the three cases where both the crystal structure (*7*, *17*, *27*) and solution NMR determined magnetic axes are available (*10*, *13*−*15*), there is a very good correlation between the direction and magnitude of the off-axis distortion of the Fe−CN unit in the crystal structure and the magnitude and direction of tilt of the major magnetic axis in solution. These data support the notion that the major magnetic axis in metMbCN complex reflects the tilt/bend with Fe−CN unit as influenced by repulsive steric (*10*) or attraction hydrogen-bonding (*14*) interactions on the distal side of the heme. Thus, the Fe−CN tilt appears to be determined primarily by distal interaction, which is in contrast to recent theoretical proposals that Fe−CO tilt/bend is controlled by proximal influences through the axial His (*8*, *63*).

Axial His Orientation and the Rhombic Magnetic Axes. Theoretically, the known His93(F8) orientation, defined by $\phi = 40°$ in Figure 1 (*5*), should produce a set of rhombic axes with angle $\kappa^* = 50°$, since the rhombic axes are related to the His plane by $90 - \phi$ (*64*, *65*). The experimentally determined value is $\kappa \approx \alpha + \gamma \approx 35 \pm 10°$. It has been shown for WT metMbCN that the residual error function (eq 2) upon determination of the magnetic axes has a very strong dependence on β, a moderate dependence on α, and only a weak dependence on γ, so that $\kappa \approx \alpha + \gamma$ is least well-defined and an uncertainty of ±10° is associated with its determination by solution NMR (*10*). The reason for this weak dependence on γ is that, primarily, residues near the heme periphery are influenced by the rhombic part of eq 1, and the size of the heme precludes close approach of such residues to the iron.

The $\cos^2 \Omega$ dependence in eq (1) demands that the meso-Hs exhibit dipolar shifts pair the α-meso-H and γ-meso-H with bias in one direction, with the paired β-meso-H and δ-meso-H shift biased in the opposite direction. While the meso-H experiences both contact and dipolar shifts, the observed asymmetry in the meso-H hyperfine shift, $\Delta\delta_{meso}$(obs), defined as

$$\Delta\delta_{meso}(\text{obs/calc}) = \frac{1}{2}[\delta_\alpha(\text{obs/calc}) - \delta_\beta(\text{obs/calc}) + \delta_\gamma(\text{obs/calc}) - \delta_\delta(\text{obs/calc})] \quad (4)$$

is quantitataively predicted by the predicted rhombic dipolar shifts, $\Delta\delta_{meso}$(calc), as has been observed for other low-spin ferrihemoproteins (*18*, *66*), which leads to the conclusion that the contact shifts for the four meso-Hs are similar, and that the observed asymmetry, $\Delta\delta_{meso}$(obs), is determined predominantly by the rhombic dipolar shifts. Hence, changes in the orientation of the in-plane magnetic axes should lead to readily observable changes in the meso-H shift index given by eq 4.

It is noted that, for WT metMbCN, the α- and γ-meso-H resonate upfield of the β- and δ-meso-Hs. The experimental $\Delta_{\delta meso}$(obs) = 2.1 ppm is in relatively good agreement with δ_{meso}(calc) = 1.8 ppm for the determined $\kappa = \sim 35°$ for WT. Consideration of the meso-H hyperfine shifts and the experimental rhombic magnetic axes for S92A-metMbCN shows a similar magnitude but with a *sign change*, $\Delta\delta_{meso}$(obs) = −1.75 ppm, relative to WT. The change in sign demands that κ increases (rhombic axes rotate counterclockwise) while the axial His plane rotates clockwise. The $\Delta\delta_{meso}$(obs) = −1.75 is adequately reproduced by a 10° increase in κ [$\Delta\delta_{meso}$(calc) = −1.65] for S92A-metMbCN. Since the κ determined by the magnetic axes necessarily has a significant uncertainty (±10°) due to the insensitivity of F/n to γ in eq 2, we consider the κ predicted by the meso-H shift pattern, as reflected in eq 4, an additional valuable indicator of the location of the rhombic magnetic axes. Hence, the *rhombic axes clearly rotates counterclockwise* by ~10° in Figure 1 on going from WT ($\kappa = 30°$) to S92A- or S92P-metMbCN ($\kappa = 40°$), in response to the axial His93(F8) imidazole plane rotating clockwise by ~10°, as expected (*26*, *64*−*67*).

In the case of H97F-metMbCN, the experimental rhombic magnetic axes provide a κ that is indistinguishable from the value for WT metMbCN. The observed heme methyl shift spread for this mutant, however, is larger than that in WT (Table 2), suggesting that the orbital hole has rotated slightly clockwise due to the rotation of the heme. The $\Delta\delta_{meso}$(obs) = 2.9 for H97F-metMbCN is larger than the 2.1 value for WT, and is consistent with the prediction that the rhombic axes have rotated *counterclockwise relative to the heme*. A plot of $\Delta\delta_{meso}$(calc) versus κ indicates a gradient of 2.5 ppm per 10° (not shown), rotation such that its 0.7 ppm increase in $\Delta\delta_{meso}$(obs) confirms that the heme has rotated clockwise by ~3°; this value is consistent with the estimates for the heme rotation deduced from the increased NOE between 8-CH_3 and Ala71(E14) $C_\beta H_3$ or Val68(E11) $C_\alpha H$.

It is noted that, while the present ^{1}H NMR data directly confirm the predicted counter-rotation of the axial His plane and rhombic axes, the value for κ differs from that predicted from $90 - \phi$. This result would suggest that, while the axial His orientation is the major factor, it is not the only determinant of the orbital ground state and rhombic axes. The electronic influence on the in-plane asymmetry due to two variably oriented vinyl groups, as well as heme π−π interaction with His97(FG3) and Phe43(CD1) are likely other

contributing factors. Last, the pattern of meso-H shifts, as influenced primarily by the rhombic dipolar shift asymmetry, provides a completely independent indicator of the location of the in-plane magnetic axes that agrees well with the values obtained from the least-squares search for α, β, and γ. Hence, *changes in the pattern of the meso-H shifts* introduced by a protein perturbation, provide a valuable empirical indicator of the rotation of the orbital hole (rhombic axes) that is complementary to that of the spread of the contact shifted heme methyl signals (*23*, *25*, *26*, *52*) in comparing the electronic structure and magnetic axes among structurally uncharacterized low-spin ferric hemoproteins.

ACKNOWLEDGMENT

The authors are indebted to Drs. J. S. de Ropp and W. Zhang for experimental assistance and valuable discussions.

SUPPORTING INFORMATION AVAILABLE

Four figures (upfield portions of TOCSY and NOESY spectra of S92A-metMbCN; schematic representation of heme cavity dipolar connections; 1:1 spectra of WT and S92-metMbCN; NMR spectra of WT and mutant metMbH_2O complexes as a function of pH) (4 pages). Ordering information is given on any masthead page.

REFERENCES

1. Dickerson, R. E., and Geis, I. (1969) *The Structure and Action of Proteins*, Harper and Row, New York.
2. Springer, B. A., Sligar, S. G., Olson, J. S., and Phillips, G. N., Jr. (1994) *Chem. Rev. 94*, 699−714.
3. Collman, J. P., Brauman, J. I., Halbert, T. R., and Suslick, K. (1976*) Proc. Natl. Acad. Sci. U.S.A. 73*, 3333−3337.
4. Cheng, X., and Schoenborn, B. P. (1991) *J. Mol. Biol. 220*, 381−399.
5. Kuriyan, J., Wilz, S., Karplus, M., and Petsko, G. A. (1986) *J. Mol. Biol. 192*, 133−154.
6. Baldwin, J. M. (1980) *J. Mol. Biol. 136*, 103−128.
7. Steigemann, W., and Weber, E. (1979) *J. Mol. Biol. 127*, 309−338.
8. Jewsbury, P., Yamamoto, S., Minato, T., Saito, M., and Kitagawa, T. (1995) *J. Phys. Chem. 99*, 12677−12685.
9. Emerson, S. D., and La Mar, G. N. (1990) *Biochemistry 29*, 1557−1566.
10. Rajarathnam, K., La Mar, G. N., Chiu, M. L., and Sligar, S. G. (1992) *J. Am. Chem. Soc. 114*, 9048−9058.
11. Rajarathnam, K., Qin, J., La Mar, G. N., Chiu, M. L., and Sligar, S. G. (1993) *Biochemistry 32*, 5670−5680.
12. Rajarathnam, K., Qin, J., La Mar, G. N., Chiu, M. L., and Sligar, S. G. (1994) *Biochemistry 33*, 5493−5501.
13. Qin, J., La Mar, G. N., Ascoli, F., and Brunori, M. (1993) *J. Mol. Biol. 231*, 1009−1023.
14. Qin, J., La Mar, G. N., Cutruzzola, F., Allocatelli, C. T., Brancaccio, A., and Brunori, M. (1993) *Biophys. J. 65*, 2178−2190.
15. Zhao, X., Vyas, K., Nguyen, B. D., Rajarathnam, K., La Mar, G. N., Li, T., Phillips Jr., G. N., Eich, R. F., Olson, J. S., Ling, J., and Bocian, D. F. (1995) *J. Biol. Chem. 270*, 20763−20774.
16. Peng, S.-M., and Ibers, J. A. (1976) *J. Am. Chem. Soc. 98*, 8032−8036.
17. Bisig, D. A., Di Iorio, E. E., Diederichs, K., Winterhalter, K. H., and Pionteck, K. (1995) *J. Biol. Chem. 270*, 20754−20762.
18. Wu, Y., Basti, M., Chiancone, E., Ascoli, F., and La Mar, G. N. (1996) *Biochim. Biophys. Acta 1298*, 261−275.
19. Satterlee, J. D. (1986) *Annu. Rep. NMR Spectrosc. 17*, 79−178.
20. Bertini, I., Turano, P., and Vila, A. J. (1993) *J. Chem. Rev. 93*, 2833−2932.
21. Lecomte, J. T. J., and La Mar, G. N. (1987) *J. Am. Chem. Soc. 109*, 7219−7220.
22. Zhang, W., La Mar, G. N., and Gersonde, K. (1996) *Eur. J. Biochem. 237*, 841−853.
23. Shulman, R. G., Glarum, S. H., and Karplus, M. (1971) *J. Mol. Biol. 57*, 93−115.
24. Traylor, T. G., and Berzinis, A. P. (1980) *J. Am. Chem. Soc. 102*, 2844−2846.
25. Banci, L., Pierattelli, R., and Turner, D. L. (1995) *Eur. J. Biochem. 232*, 522−527.
26. Turner, D. L. (1995) *Eur. J. Biochem. 227*, 829−837.
27. Bolognesi, M., Coda, A., Frigerio, F., Gatti, G., Ascenzi, P., and Brunori, M. (1990) *J. Mol. Biol. 225*, 621−625.
28. Kolczak, U., Han, C., Silvia, L. A., and La Mar, G. N. (1997) *J. Am. Chem. Soc. 119*, 12643−12654.
29. Smerdon, S. J., Krzywda, S., Wilkinson, A. J., Brantley, R. E., Jr., Carver, T. E., Hargrove, M. S., and Olson, J. S. (1993) *Biochemistry 32*, 5132−5138.
30. Shiro, Y., Iizuka, T., Marubayashi, K., Ogura, T., Kitagawa, T., Balasubramanian, S., and Boxer, S. G. (1994) *Biochemistry 33*, 14986−14992.
31. Springer, B. A., and Sligar, S. G. (1987) *Proc. Natl. Acad. Sci. U.S.A. 84*, 8961−8965.
32. Phillips, G. N., Jr., Arduini, R. M., Springer, B. A., and Sligar, S. G. (1990) *Proteins: Struct., Funct., Genet. 7*, 358−365.
33. Abadan, Y., Chien, E. Y. T., Chu, K., Eng, C. D., Nienhaus, G. U., and Sligar, S. G. (1995) *Biophys. J. 68*, 2497−2504.
34. Rohlfs, R. J., Mathews, A. J., Carver, T. E., Olson, J. S., Springer, B. A., Egeberg, K. D., and Sligar, S. G. (1990) *J. Biol. Chem. 265*, 3168−3176.
35. Inubushi, T., and Becker, E. D. (1983) *J. Magn. Reson. 51*, 128−133.
36. Emerson, S. D., and La Mar, G. N. (1990) *Biochemistry 29*, 1545−1556.
37. Plateau, P. and Gueron, M. (1982) *J. Am. Chem. Soc. 104*, 7310−7311.
38. Bax, A. (1984) *Two-dimensional Nuclear Magnetic Resonance in Liquids*, D. Reidell Publishing Company, London, U.K.
39. Jeener, J., Meier, B. H., Bachmann, P., and Ernst, R. R. (1979) *J. Chem. Phys. 71*, 4546−4553.
40. Griesinger, C., Otting, G., Wüthrich, K., and Ernst, R. R. (1988) *J. Am. Chem. Soc. 110*, 7870−7872.
41. Dalvit, C. and Wright, P. E. (1987) *J. Mol. Biol. 194*, 313−327.
42. Theriault, Y., Pochapsky, T. C., Dalvit, C., Chiu, M. L., Sligar, S. G., and Wright, P. E. (1994) *J. Biomol. NMR 4*, 491−504.
43. Bondi, A. and Wüthrich, K. (1979) *Biopolymers 18*, 285−297.
44. Wüthrich, K. (1986) *NMR of Proteins and Nucleic Acids*, Wiley, New York.
45. Wishart, D. S., Sykes, B. D. and Richards, F. (1991) *J. Mol. Biol. 222*, 311−333.
46. Cross, K. J., and Wright, P. E. (1985) *J. Magn. Reson. 64*, 220−231.
47. Antonini, E., and Brunori, M. (1971) *Hemoglobin and Myoglobin and Their Reactions with Ligands*, North-Holland Publishing Company, Amsterdam, pp 40−54.
48. Berzofsky, J. A., Peisach, J., and Alben, J. O. (1972) *J. Biol. Chem. 247*, 3774−3782.
49. Lloyd, E., and Mauk, A. G. (1994) *FEBS Lett. 340*, 281−286.
50. Chatfield, M. J., La Mar, G. N., Smith, K. M., Leung, H.-K., and Pandey, R. K. (1988) *Biochemistry 27*, 1500−1507.
51. Berzofsky, J. A., Peisach, J., and Blumberg, W. E. (1971) *J. Biol. Chem. 246*, 3367.
52. Qin, J., and La Mar, G. N. (1992) *J. Biomol. NMR 2*, 597−618.
53. Yamamoto, Y., Nanai, N., Chujo, R., and Suzuki, T. (1990) *FEBS Lett. 264*, 113−116.
54. Tilton, R. F., Kuntz, I. D., and Petsko, G. A. (1984) *Biochemistry 23*, 2849−2857.
55. Krishnamoorthi, R., and La Mar, G. N. (1984) *Eur. J. Biochem. 138*, 135−140.

56. Cutnell, J. D., La Mar, G. N., and Kong, S. B. (1981) *J. Am. Chem. Soc. 103*, 3567−3572.
57. La Mar, G. N., Budd, D. L., Smith, K. M., and Langry, K. C. (1980) *J. Am. Chem. Soc. 102*, 1822−1827.
58. Takano, T. (1977) *J. Mol. Biol. 110*, 537−568.
59. McGrath, T. M., and La Mar, G. N. (1978) *Biochim. Biophys. Acta 534*, 99−111.
60. Scheidt, W. R., and Chipman, D. M. (1986) *J. Am. Chem. Soc. 108*, 1163−1167.
61. Perutz, M. F. (1970) *Nature (London) 228*, 726−739.
62. Lloyd, E., Burk, D. L., Ferrer, J. C., Maurus, R., Doran, J., Carey, P. R., Brayer, G. D., and Mauk, A. G. (1996) *Biochemistry 35*, 11901−11912.
63. Jewsbury, P., Yamamoto, S., Minato, T., Saito, M., and Kitagawa, T. (1994) *J. Am. Chem. Soc. 116*, 11586−11587.
64. Oosterhuis, W. T., and Lang, G. (1969) *Phys. Rev. 178*, 439−456.
65. Byrn, M. P., Katz, B. A., Keder, N. L., Levan, K. R., Magurany, C. J., Miller, K. M., Pritt, J. W., and Strouse, C. E. (1983) *J. Am. Chem. Soc. 105*, 4916−4922.
66. Lee, K.-B., La Mar, G. N., Mansfield, K. E., Smith, K. M., Pochapsky, T. C., and Sligar, S. G. (1993) *Biochim. Biophys. Acta 1202*, 189−199.
67. Shokhirev, N. V., and Walker, F. A. (1998) *J. Am. Chem. Soc.* (in press).

BI9728295